



Butler University Digital Commons @ Butler University

Scholarship and Professional Work - LAS

College of Liberal Arts & Sciences

2007


Phase diagram of the one-dimensional Hubbard-Holstein model at half and quarter filling

Rahul Hardikar

Butler University, rhardika@butler.edu

R. T. Clay

Follow this and additional works at: http://digitalcommons.butler.edu/facsch_papers

 Part of the [Atomic, Molecular and Optical Physics Commons](#), and the [Quantum Physics Commons](#)

Recommended Citation

Hardikar, Rahul and Clay, R. T., "Phase diagram of the one-dimensional Hubbard-Holstein model at half and quarter filling" *Physical Review B* / (2007): -.

Available at http://digitalcommons.butler.edu/facsch_papers/820

This Article is brought to you for free and open access by the College of Liberal Arts & Sciences at Digital Commons @ Butler University. It has been accepted for inclusion in Scholarship and Professional Work - LAS by an authorized administrator of Digital Commons @ Butler University. For more information, please contact fgaede@butler.edu.

Phase diagram of the one-dimensional Hubbard-Holstein model at half and quarter filling

R. P. Hardikar and R. T. Clay^{1,*}

¹*Department of Physics and Astronomy and HPC Center for Computational Sciences, Mississippi State University, Mississippi State, Mississippi 39762, USA*

(Received 11 December 2006; revised manuscript received 4 April 2007; published 6 June 2007)

The Hubbard-Holstein model is one of the simplest to incorporate both electron-electron and electron-phonon interactions. In one dimension at half filling, the Holstein electron-phonon coupling promotes on-site pairs of electrons and a Peierls charge-density wave, while the Hubbard on-site Coulomb repulsion U promotes antiferromagnetic correlations and a Mott insulating state. Recent numerical studies have found a possible third intermediate phase between Peierls and Mott states. From direct calculations of charge and spin susceptibilities, we show that (i) as the electron-phonon coupling is increased, first a spin gap opens, followed by the Peierls transition. Between these two transitions, the metallic intermediate phase has a spin gap, no charge gap, and properties similar to the negative- U Hubbard model. (ii) The transitions between Mott/intermediate and intermediate/Peierls states are of the Kosterlitz-Thouless form. (iii) For larger U , the two transitions merge at a tricritical point into a single first-order Mott/Peierls transition. In addition, we show that an intermediate phase also occurs in the quarter-filled model.

DOI: 10.1103/PhysRevB.75.245103

PACS number(s): 71.10.Fd, 71.30.+h, 71.45.Lr

I. INTRODUCTION

In crystalline materials where one or more of the building blocks of the crystal structure is a large molecule, the vibrational properties of the molecules often have large effects on the overall electronic properties of the material. One large family of such molecular crystalline materials are the organic conductors and superconductors.¹ While some molecular crystals such as the fullerene superconductors² have a three-dimensional crystal structure, many other examples are either quasi-one- or quasi-two-dimensional, i.e., charge transport is restricted in certain directions due to anisotropic crystal structure. In addition to strong electron-phonon (e-ph) coupling to the molecular vibrations, electron-electron (e-e) interactions are often important in low dimensional materials. In this paper, we present numerical calculations of the phase diagram for one of the simplest possible many-body models incorporating both these effects, the Hubbard-Holstein model (HHM) in one dimension (1D). In the HHM, internal (intramolecular) molecular vibrations are coupled to the local charge density of the electrons.³ The electrons further interact with other electrons with an onsite Coulomb repulsion when two electrons occupy the same orbital.⁴ Surprisingly, complex effects result from this simple model due to the presence of both e-e and e-ph interactions.

The 1D HHM Hamiltonian we consider is

$$H = -t \sum_{j,\sigma} (c_{j+1,\sigma}^\dagger c_{j,\sigma} + \text{H.c.}) + U \sum_j n_{j,\uparrow} n_{j,\downarrow} + g \sum_{j,\sigma} (a_j^\dagger + a_j) n_{j,\sigma} + \omega \sum_j a_j^\dagger a_j, \quad (1)$$

where $c_{j,\sigma}^\dagger (c_{j,\sigma})$ are creation (annihilation) operators for electrons on site j with spin σ , $a_j^\dagger (a_j)$ are bosonic creation (annihilation) operators for phonons at site j , and the electron number operator $n_{j,\sigma} = c_{j,\sigma}^\dagger c_{j,\sigma}$. U is the Hubbard on-site e-e interaction energy, ω is the dispersionless phonon frequency, and g is the e-ph coupling constant. All energies in this paper will be given in units of t , the electron hopping integral.

We will concentrate primarily on Eq. (1) in the half-filled band limit (one electron per lattice site), but also discuss briefly the quarter-filled band (one electron per two lattice sites). The effect of e-ph interactions on a half-filled 1D metal is well known: for inter-molecular phonons corresponding to the relative motion of adjacent molecules in the crystal, the 1D lattice dimerizes with alternating strong and weak bonds. In this bond-order wave (BOW) state, the expectation value of the electron hopping between adjacent sites alternates between strong and weak values. The dimerized chain then has a gap at the Fermi level and an insulating ground state.⁵ This Peierls state has both charge and spin gaps, and a bond modulation at $2k_F$ ($q = \pi$) at half filling. For Holstein-type phonons that couple to the local charge density, a similar Peierls state occurs, but instead of bond deformation, the local charge density is modulated in a charge-density wave (CDW) ground state. The CDW Peierls state at half filling has alternating large and small charge densities again with periodicity $2k_F$. Similarly, the effect of the Hubbard on-site interaction in 1D is well known: for any $U > 0$ at half filling, the ground state is an insulator.⁶ Antiferromagnetic (AFM) spin correlations are present in this Mott insulating state, although no long-range antiferromagnetic order is possible in 1D. At half filling, the $2k_F$ CDW cannot coexist with $2k_F$ AFM correlations and hence the Peierls and AFM states are competing.

Numerous previous studies have examined HHM within various approximations and analytic or numerical techniques. In the limit $\omega \rightarrow \infty$, one can integrate out the phonons leaving an effective U composed of the sum of the Hubbard U and the effective phonon interaction, $U_{\text{eff}} = U - 2g^2/\omega$. For $U_{\text{eff}} > 0$, one expects the Mott state, while for $U_{\text{eff}} < 0$, one expects the Peierls state.^{7,8} If the phonons are treated in the classical (adiabatic $\omega \rightarrow 0$) limit, one expects Peierls order for any $g > 0$ at $U = 0$. However, it was shown in the spinless model [Eq. (1) with a single species of fermion] that quantum fluctuations of the phonon field lead to a finite e-ph coupling g_c before the Peierls state is formed at $U = 0$.⁷⁻⁹ The

model with spin [Eq. (1)] has since been shown to also require a finite e-ph coupling for the Peierls transition.^{10,11}

In addition to studies of the 1D model, several recent studies have been performed on the Holstein and HHM in the limit of infinite dimensions ($d=\infty$) using dynamical mean-field theory (DMFT) and related methods.^{12–14} In the $d=\infty$ model, the system is metallic at $U=0$ also for g less than a finite value. However, an important distinction between $d=\infty$ results and those presented here is that at $d=\infty$, the Mott insulating transition occurs at a finite value of U , $U \gtrsim 6t$, while at $d=1$, it occurs for $U > 0$. Some similarities are found with our results, in particular, that there is a deviation in the critical coupling for the Peierls transition from $U_{\text{eff}}=0$ at small U .¹⁴

Given that in the half-filled 1D HHM at $U=0$ the ground state is metallic (no charge gap and a finite Drude weight) for a finite value of g , it was proposed that this metallic phase continues to exist *between* the Peierls and Mott insulating phases for $U > 0$.¹⁵ Subsequent numerical calculations confirmed that a metallic phase exists for both $U=0$ and finite U .¹⁶ In this paper, we present more detailed numerical results and analysis of the phase diagram. We confirm the intermediate phase using a different and more direct order parameter and present more detailed finite-size scaling of the quantum phase transitions. From the finite-size dependence, we determine that the two transitions (Mott/intermediate and intermediate/Peierls) are of the Kosterlitz-Thouless (KT) type. We find that for larger U , the two transitions merge into a single first-order Mott/Peierls transition. In our revised analysis, we find that the apparent presence of the Luttinger liquid (LL) exponent $K_\rho > 1$ (Ref. 16) *does not* imply dominant superconducting pairing correlations, but is more likely a finite-size effect. We present the phase diagram for three different phonon frequencies. We further show that at quarter filling, a similar intermediate phase occurs.

The outline of the paper follows. We first give some details of the numerical method we used. Turning to our results, we discuss the $U=0$ case and then move on to finite U and the quarter-filled band. Finally, we conclude with a discussion of our data and their relation to other theoretical results, as well as unanswered questions for further study.

II. METHOD

We use the stochastic series expansion (SSE) quantum Monte Carlo (QMC) method.^{17–21} SSE provides statistically exact results (no Trotter discretization of imaginary time is used) and has been adapted for many different quantum lattice models. Although this method has been described in detail elsewhere, we briefly describe here our treatment of the Holstein phonon interaction.

In SSE, the partition function $Z = \text{Tr}\{e^{-\beta H}\}$ is expanded in terms of a series of sequences S_L of operators H_{a_i, b_i} :

$$Z = \sum_{\alpha} \sum_{S_L} \frac{\beta^n (L-n)!}{L!} \left\langle \alpha \left| \prod_{i=1}^L H_{a_i, b_i} \right| \alpha \right\rangle. \quad (2)$$

In Eq. (2), n is the length (number of operators) of each sequence, L is the maximum allowed sequence length, β is

the inverse temperature, and $|\alpha\rangle$ is a basis state, here, a direct product of electron and phonon configurations. In order to obtain the ground-state phase diagram, all results presented here used $\beta/t \geq 2N$, where N is the number of lattice sites. The operators H_{a_i, b_i} define the Hamiltonian and have type (a_i) and bond (b_i) indices with i indicating their position within the sequence S_L . For the 1D Hubbard model [Eq. (1) with $g=\omega=0$], we have three different operators representing the diagonal interaction and electron hopping for both spins:¹⁷

$$H_{1,j} = C - \frac{U}{2} \left[\left(n_{\uparrow,j} - \frac{1}{2} \right) \left(n_{\downarrow,j} - \frac{1}{2} \right) + \left(n_{\uparrow,j+1} - \frac{1}{2} \right) \left(n_{\downarrow,j+1} - \frac{1}{2} \right) \right] + \mu(2 - n_j - n_{j+1}), \quad (3)$$

$$H_{2,j} = c_{j+1,\uparrow}^\dagger c_{j,\uparrow} + \text{H.c.}, \quad (4)$$

$$H_{3,j} = c_{j+1,\downarrow}^\dagger c_{j,\downarrow} + \text{H.c.} \quad (5)$$

Here, j labels the first site of the bond the operator acts on. μ is the chemical potential, written here so that $\mu=0$ corresponds to half filling. C is a constant chosen so that the expectation value of $H_{1,j}$ is always positive definite. In addition to the operators of Eqs. (3)–(5), a null operator H_0 is used as a placeholder in the sequence expansion. We represent the phonons in the phonon-number basis and add the following operators for the e-ph interactions and phonon diagonal energy:

$$H_{4,j}^L = g a_j^\dagger n_j, \quad (6)$$

$$H_{4,j}^R = g a_{j+1}^\dagger n_{j+1}, \quad (7)$$

$$H_{5,j}^L = g a_j n_j, \quad (8)$$

$$H_{5,j}^R = g a_{j+1} n_{j+1}, \quad (9)$$

$$H_{6,j} = \omega(N_p - a_j^\dagger a_j). \quad (10)$$

Additionally, for the HHM, μ in Eq. (3) should be replaced by $(2g^2/\omega + \mu)$. Since the Holstein interaction couples the electron density on a single site while the SSE operators typically act on bonds composed of two sites, we define two different phonon operators acting on phonon numbers on the left or right of the bond. These have superscripts L and R , respectively. The diagonal operator $H_{6,j}$ also acts on a single site j . N_p is a cutoff in the maximum number of phonons per site. We discuss further below the choice of this cutoff, but, in practice, it can be chosen large enough so as to not affect the accuracy of the method.

The Monte Carlo updating is composed of an update for the electrons followed by an update for the phonons. The electron update consists of an update changing the number of diagonal $H_{1,j}$ operators in the sequence, followed by a loop update that exchanges diagonal and off-diagonal operators. For the electrons, we use the directed loop algorithm.²¹ We

note that the operators [Eqs. (6)–(10)] are not changed during the electron loop update. The phonon updating also consists of two parts, first, a diagonal update changing numbers of $H_{6,j}$ operators, and second, an off-diagonal update exchanging H_1 , H_4 , and H_5 operators. In the diagonal phonon update, H_0 operators are interchanged with $H_{6,j}$ operators with the following Metropolis algorithm probabilities (N_H is the total number of non- H_0 operators present in the sequence):

$$P_{0 \rightarrow 6} = \frac{N\beta\omega(N_p - \langle a_j^\dagger a_j \rangle)}{L - N_H}, \quad (11)$$

$$P_{6 \rightarrow 0} = \frac{L - N_H + 1}{N\beta\omega(N_p - \langle a_j^\dagger a_j \rangle)}. \quad (12)$$

The phonon update for off-diagonal operators is similar to the technique described in Ref. 22. For each site in the system, a *subsequence* is constructed which is a subset of the operators in S_L . The subsequence consists of only the operators $H_{1,m}$, $H_{4,m}$, and $H_{5,m}$ which act on phonons at a particular site m . Within the subsequence, adjacent pairs of operators are then selected at random and changed with a Metropolis probability. The pair substitutions that change the phonon number are (omitting the site index m as all apply to the same site)

$$(H_1, H_1) \rightarrow (H_4, H_5), (H_5, H_4), \quad (13)$$

$$(H_4, H_5) \rightarrow (H_1, H_1), \quad (14)$$

$$(H_5, H_4) \rightarrow (H_1, H_1). \quad (15)$$

In addition, pair substitutions are attempted that swap the order in the subsequence of the two operators. When two different pairs may be substituted, the substitution made is chosen randomly. Note that the L and R indices in Eqs. (6)–(9) are not needed during the pair updating, but updates involving the H_1 operators must be canceled with 50% probability (for each H_1 operator in the pair). If a H_1 operator changes into a phonon operator as a result of the update, a L or R index is assigned when the subsequence update is completed and merged into S_L . The Metropolis substitution probabilities depend on phonon, as well as diagonal electron matrix elements variables, the e-ph coupling constant g , and the number N_d of diagonal phonon operators ($H_{6,j}$) that are present between the two operators of the pair. N_d may be stored when the subsequence is constructed. For example, in terms of just the change in the phonon part of the operator,

$$P[(H_1, H_1) \rightarrow (H_5, H_4)] = Rng^2 \left(\frac{N_p - n + 1}{N_p - n} \right)^{N_d}, \quad (16)$$

$$P[(H_5, H_4) \rightarrow (H_1, H_1)] = \frac{R}{ng^2} \left(\frac{N_p - n}{N_p - n + 1} \right)^{N_d}, \quad (17)$$

where n is the number of phonons present in the sequence position just before the operator pair. R in Eqs. (16) and (17) is the ratio of diagonal matrix elements from the electronic Hamiltonian. In practice, the number of pair substitutions

performed is chosen to be approximately the same as the number of operators in the subsequence.

We use standard methods to calculate various observables within our SSE code.¹⁷ To determine phase boundaries of the model, we primarily use the charge and spin susceptibilities at wave vector q given by

$$O_j^\pm = n_{j,\uparrow} \pm n_{j,\downarrow}, \quad (18)$$

$$\chi_{\rho,\sigma}(q) = \frac{1}{N} \sum_{j,k} e^{iq(j-k)} \int_0^\beta d\tau \langle O_j^\pm(\tau) O_k^\pm(0) \rangle. \quad (19)$$

In Eq. (19), the charge susceptibility $\chi_\rho(q)$ [spin susceptibility $\chi_\sigma(q)$] corresponds to the + (–) sign. Similarly, we also use the static structure factors $S_\rho(q)$ and $S_\sigma(q)$:

$$S_{\rho,\sigma} = \frac{1}{N} \sum_{j,k} e^{iq(j-k)} \langle O_j^\pm O_k^\pm \rangle. \quad (20)$$

The effective low-energy properties of many interacting 1D models can be understood in terms of a LL picture, and the asymptotic properties of the system described by a small number of parameters.^{23,24} In particular, the asymptotic decay of correlation functions can be related to the correlation exponents K_ρ and K_σ for charge and spin, respectively. In the long-wavelength limit, these exponents may be calculated from the slope of the structure factors

$$K_{\rho,\sigma} = \pi \lim_{q \rightarrow 0} S_{\rho,\sigma}(q)/q. \quad (21)$$

In practice, one uses the behavior of $\pi S(q)/q$ at the smallest available q for the periodic ring, $q_1 = 2\pi/N$. With proper finite-size scaling in N , this gives the Luttinger liquid exponent for the system.²⁵ Based on calculations of acoustic phonons coupled to 1D electrons, it has been suggested that the expected relationship of K_ρ to the correlation functions must be modified in the presence of phonon interactions with retardation.^{26–28} We will discuss this further in Sec. III D below. However, we note that the interpretation of K_σ is *not* modified in the presence of phonon retardation effects since spin-rotation symmetry is preserved in the HHM. K_σ is expected to be exactly equal to 1 unless a spin gap is present, and the condition that $\pi S_\sigma(q_1)/q_1$ decreases below 1 is a sensitive indicator for the opening of a spin gap (see Fig. 1).²⁰ We find that finite-size effects in determining the phase boundaries using Eq. (21) are worse than when using the susceptibilities, Eq. (19), due to the necessity of taking the limit $q_1 \rightarrow 0$ in Eq. (21). Therefore, we will primarily use the susceptibilities in order to determine the phase diagram boundaries.

We choose the phonon cutoff N_p such that phonon occupation numbers during the simulation never reach within some fraction ($\sim 20\%$) of the cutoff, similar to the method in which the maximum sequence length L is set self-consistently in SSE simulations. We have verified that our results are converged with respect to N_p . Typical variation with N_p is shown in Fig. 1 for a 16 site system with $U=4$ and $\omega=1$. We find that choosing too small N_p can have a noticeable effect on the critical coupling for transitions and especially on quantities measured in the Peierls phase.

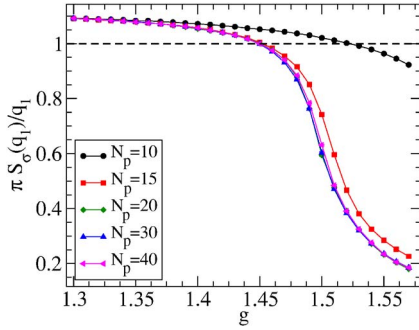


FIG. 1. (Color online) Slope of the spin structure factor at wave vector $q_1=2\pi/N$ versus e-ph coupling g for a 16 site half-filled system with $U=4$ and $\omega=1$. $\pi S_\sigma(q_1)/q_1$ crossing 1 indicates the opening of a spin gap. Different symbols show the convergence with increasing phonon cutoff N_p .

Autocorrelation time τ is an important measure of the overall efficiency of a Monte Carlo method. Correlations between measurements are typically found to decay as $\sim e^{-t/\tau}$, where t is in units of Monte Carlo time corresponding to the number of updating steps completed. If measurements are correlated, the estimated statistical error must be increased. In general, it is found that near quantum phase transitions, τ often increases steeply, making calculations near phase boundaries difficult or impossible. One tool available to improve QMC calculations near phase boundaries is quantum parallel tempering.²⁹ In this technique, separate processors on a parallel computer have slightly different parameter values. Periodically, a Metropolis move is attempted to switch the configuration between adjacent processors. These moves help to prevent the algorithm from getting “stuck” in one configuration and consequently reduce the autocorrelation time. In Fig. 2, we show the integrated autocorrelation time for long-wavelength structure factor measurements [Eq. (21)], defined as in Ref. 21. Our definition of one Monte Carlo step is similar to Ref. 21, with an average $2N_H$ loop

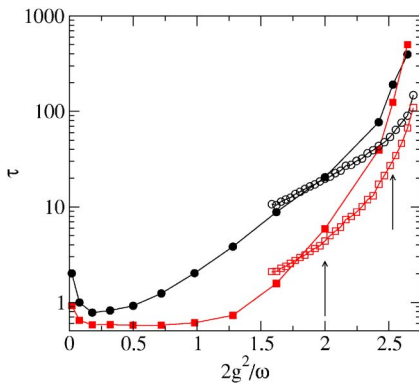


FIG. 2. (Color online) Integrated autocorrelation time for $N=16$, $U=2$, $\omega=1$, $\beta=32$, and $N_p=30$ as a function of e-ph coupling. Filled circles (squares) are the autocorrelation time for the charge (spin) structure factor $S(q_1)$ at $q_1=2\pi/N$. Open symbols are for the same observables, but calculated using quantum parallel tempering. Arrows indicate the location of the two transitions (see Sec. III). We find that parallel tempering significantly reduces the autocorrelation time near the transitions.

vertices visited in the electronic loop update. As expected, we find that τ increases greatly near the Peierls transition. We also find that parallel tempering decreases the autocorrelation time significantly and is essential to obtain reliable results near the Peierls transition.

III. RESULTS AT HALF FILLING

We first present our results for the half-filled band, first in the case $U=0$ and then for finite U .

A. $U=0$: The Peierls transition

Equation (1) has been studied in great detail for the case of $U=0$. One of the key questions is whether the transition to the Peierls state occurs for finite critical coupling or for any value of $g>0$. The transition occurring at finite g is expected to be of the KT type.^{7,30} KT transitions at finite phonon coupling have been found in a number of 1D phonon-coupled models including the spinless Holstein model [Eq. (1) with only one species of fermion],^{7,9} the XY model coupled to dispersionless phonons,³¹ the Heisenberg model coupled to dispersionless phonons,¹⁹ and the extended Peierls-Hubbard model coupled to dispersionless bond phonons.²⁰ We confirm that indeed a finite critical coupling exists and show that the finite-size scaling of the observables is consistent with a KT transition.

A KT quantum phase transition is difficult to detect because the gap opens exponentially slowly. For Holstein-type phonons that couple to the local electron density, the appropriate order parameter for the transition is the $2k_F$ charge susceptibility. The critical coupling (we will denote the critical g for the Peierls transition as g_{c2}) may be determined from the finite-size scaling of the $2k_F$ charge susceptibility $\chi_\rho(\pi)$. $\chi_\rho(\pi)/N$ should approach zero logarithmically below g_{c2} and should diverge above g_{c2} . Exactly at $g=g_{c2}$, log corrections vanish and $\chi_\rho(\pi)/N$ should approach a constant value with increasing N . Our SSE results confirm that $\chi_\rho(\pi)$ does scale in this manner. In Fig. 3(a), we show charge susceptibility data for $U=0$ and $\omega=1$, which is consistent with a KT transition at $g_{c2}\approx 0.7$. We see a clear decrease of $\chi_\rho(\pi)/N$ with system size below the transition and a clear increase above the transition. Plotted as a function of effective e-ph coupling $2g^2/\omega$ [Fig. 3(b)], $\chi_\rho(\pi)/N$ for different N cross at the transition. In Fig. 3(b), we show a finite-size scaling of the transition point obtained by plotting value of $2g^2/\omega$ where the susceptibility curve for N sites intersects the data for $N/2$ sites. We find that these intersection points are well fitted to a linear dependence in $1/N$, giving $2g_{c2}^2/\omega=1.00$ for $U=0$.

In Fig. 4, we show for comparison the long-wavelength charge and spin structure factor slopes, Eq. (21), which are estimates for the LL exponents K_ρ and K_σ . For any $g>0$, K_σ is less than 1 and decreases with increasing chain length, indicating a spin gap. Furthermore, in the spin susceptibility (not shown here), we find no sign of any transition at the critical coupling where $\chi_\rho(\pi)/N$ diverges. We denote the critical coupling for the spin gap opening as g_{c1} . Hence, we conclude that a spin gap is present for *any* $g>g_{c1}=0$ when

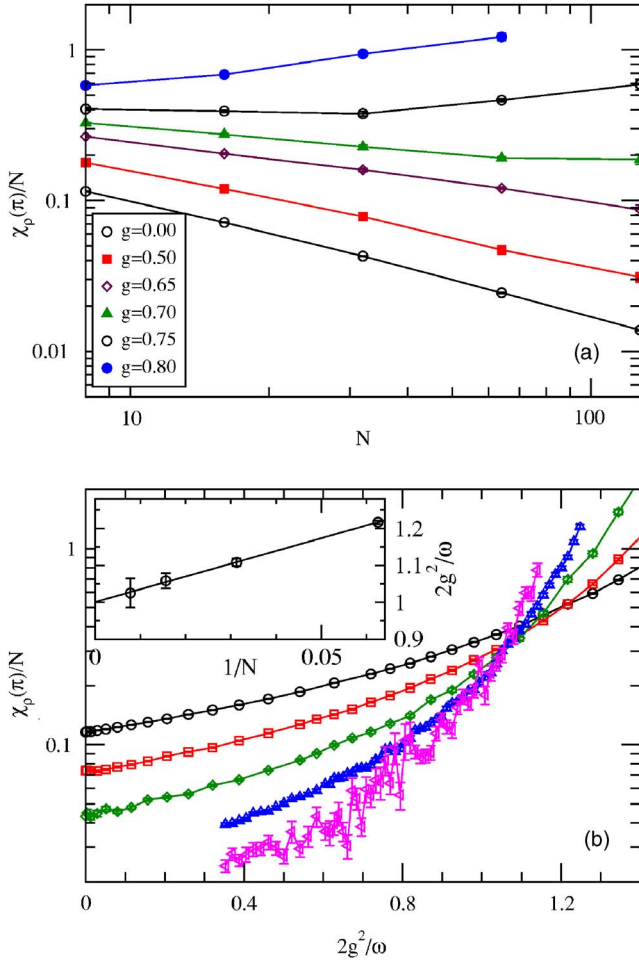


FIG. 3. (Color online) Finite-size scaling of the $q=\pi$ charge susceptibility for $U=0$ and $\omega=1$ at half filling. Data are for system sizes up to $N=128$ sites. In (a), we plot $\chi_\rho(\pi)/N$ versus N . At critical coupling, $\chi_\rho(\pi)/N$ approaches a constant for large N . Note that the $g=0$ curve corresponds to free fermions (no phonons). In (b), $\chi_\rho(\pi)/N$ is plotted versus the effective e-ph coupling $2g^2/\omega$, for system sizes $N=8$ (open circles), 16, 32, 64, and 128. The inset shows finite-size scaling of the transition point obtained by plotting the value of $2g^2/\omega$ where $\chi_\rho(\pi)/N$ for system size N exceeds the susceptibility for system size $N/2$. Line in the inset is a linear fit. We estimate the critical coupling as $2g_{c2}^2/\omega \approx 1.00$ ($g_{c2} \approx 0.71$).

$U=0$, but a charge gap is only present for $g > g_{c2}$. In the inset of Fig. 4, we show the finite-size scaling of point where $K_\rho = 1$ ($2g_{c2}^2/\omega$). We discuss further the K_ρ data in Sec. III D and the apparent small discrepancy between g_{c2} determined from susceptibility versus K_ρ data.

B. $U > 0$: Intermediate phase

We next consider the case with $U > 0$ at half filling. To avoid any possible difficulties of interpreting numerical estimates for K_ρ , we determine all phase boundaries *directly from susceptibilities* and K_σ . In the 1D Hubbard model [$g=0$ in Eq. (1)], charge and spin degrees of freedom effectively switch places at $U=0$. In terms of the susceptibilities, $\chi_\rho(\pi)$ and $\chi_\sigma(\pi)$ are exactly equal at $U=0$.

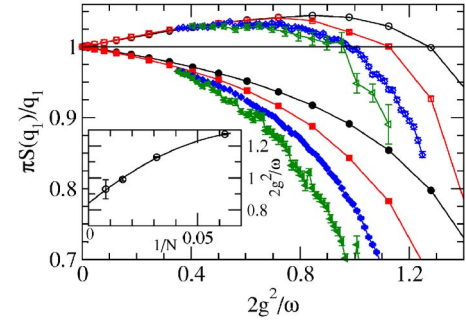


FIG. 4. (Color online) Long-wavelength spin and charge structure factor slopes for $U=0$ and $\omega=1$ at half filling. Open (filled) symbols are for charge (spin). Data are for system sizes of $N=16$, 32, 64, and 128 sites. For any $g > 0$, $\pi S_\rho(q_1)/q_1$ is less than 1 indicating the presence of a spin gap. The inset shows the finite-size scaling of the point where $S_\rho(q_1)/q_1$ crosses 1, with the line a fit to a quadratic. We estimate the critical coupling as $2g_{c2}^2/\omega \approx 0.85$. The appearance of these data for $g < g_{c2}$ is similar to those for the negative- U Hubbard model (Fig. 7 for $U < 0$). The interpretation of these data is discussed in Sec. III D.

In Fig. 5(a), we first show the $2k_F$ charge and spin susceptibilities for $U=2$ and $\omega=1$. We find that when $U_{\text{eff}} \approx 0$ ($g=1$ for $U=2$ and $\omega=1$), the charge and spin susceptibilities become equal as in the simple Hubbard case. The estimate for K_σ , shown in Fig. 5(b), again crosses 1 indicating an opening of a spin gap. This transition is therefore the same transition g_{c1} as discussed above in Sec. III A, but now occurring at finite g . The quantum phase transition as g increases past g_{c1} appears identical to the transition as U becomes negative in the 1D Hubbard model. Based on the similarity with the 1D Hubbard model, we conclude that the spin-gap transition here is also of the KT form.

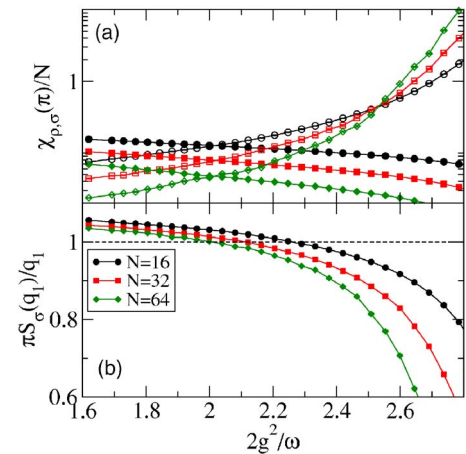


FIG. 5. (Color online) (a) Charge (open symbols) and spin (filled symbols) susceptibilities for the half-filled HHM with $U=2$, $\omega=1$. The first transition (g_{c1}) occurs where $\chi_\rho = \chi_\sigma$ corresponding to $U_{\text{eff}}=0$. The second transition (g_{c2}) is the Peierls transition, where $\chi_\rho(\pi)/N$ diverges as in Fig. 3. Note that the spin susceptibility is also divided by N to make the crossing at $U_{\text{eff}}=0$ clear. (b) Long-wavelength spin structure factor for $U=2$, $\omega=1$. The point where $\pi S_\rho(q_1)/q_1$ crosses unity indicates the opening of the spin gap, identical to the point where $\chi_\rho = \chi_\sigma$ in (a).

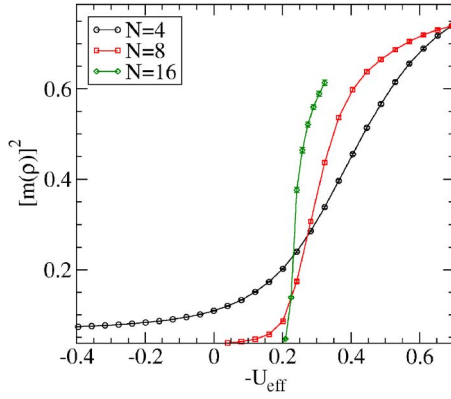


FIG. 6. (Color online) First-order Mott/Peierls transition for large U . We show the CDW order parameter $[m(\rho)]^2$ (see text) vs $-U_{\text{eff}}=2g^2/\omega-U$ for $\omega=1$ and $U=8$. The Mott/Peierls transition occurs for $U_{\text{eff}} \sim -0.2$.

In Fig. 5(a), a second transition takes place beyond the spin-gap transition at g_{c1} . This second transition is again the Peierls transition indicated by the divergence of $\chi_\rho(\pi)/N$. Beyond the second transition point ($g > g_{c2}$), $\chi_\rho(\pi)/N$ increases with increasing system size, and as in Fig. 3(b) $\chi_\rho(\pi)/N$ for different system sizes cross at $g=g_{c2}$ when plotted versus e-ph coupling. For $g_{c1} < g < g_{c2}$, we now have a third intermediate phase, which has a spin gap but no Peierls order. In Fig. 5(a), we see only very small finite-size effects in determining g_{c1} and g_{c2} from the susceptibility data. The g_{c1} from our data shows little deviation from $U_{\text{eff}}=0$, at least for small to intermediate U as compared to ω . Finite-size effects are more significant in K_σ as estimated from the spin structure factor slope in Fig. 5(b) because $q_1=2\pi/N$ only approaches $q_1=0$ in the limit $N \rightarrow \infty$. However, for increasing N , g_{c1} as estimated from K_σ does converge to the same value we obtain from the susceptibility.

As U increases, we find that two transitions at g_{c1} and g_{c2} occur closer together, becoming indistinguishable from each other at approximately $U \sim 5$ for $\omega=1$. At this point and for larger U , the two KT transitions merge into a single Mott/Peierls transition. We next show that this merged transition is *first order*.

C. First-order transition

Above a critical U value $U=U_m$, we find that the spin-gap and Peierls transitions coincide. The phase diagram then has a shape very similar to that of the half-filled 1D extended Hubbard model (EHM).^{29,32–34} In the half-filled EHM, as the nearest-neighbor Coulomb repulsion V is increased for fixed U , there is a transition from AFM to CDW order. This transition is continuous for small U and first order for $U > U_m$. In a first-order quantum phase transition, observables become discontinuous as one of the Hamiltonian parameters is varied. For the HHM, a change to first-order behavior for strong coupling has also been seen in DMFT studies.¹⁴ As in Ref. 29, we take $[m(\rho)]^2=S_\rho(\pi)/N$ as an order parameter for the Peierls CDW state. We show in Fig. 6 $[m(\rho)]^2$ for $U=8$ and $\omega=1$. We find a sharp jump in $[m(\rho)]^2$ at the transition with

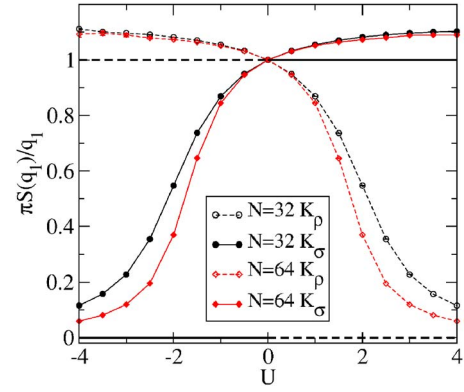


FIG. 7. (Color online) LL exponents for the 1D Hubbard model [Eq. (1) with $g=0$] estimated from the long-wavelength charge and spin correlations. K_ρ (K_σ) is given by open (filled) symbols. In the infinite N limit, $K_\rho=1$ for any $U < 0$ and $K_\rho=0$ for $U > 0$; $K_\sigma=1$ for any $U > 0$ and $K_\sigma=0$ for any $U < 0$. Observing these limiting values (shown by full and dashed horizontal lines) is difficult due to finite value of $q_1=2\pi/N$ and also the logarithmic scaling with N for the exponent whose value is unity.

the discontinuity becoming stronger for larger system sizes. Other observables such as the ground-state energy and bond order also show discontinuous behavior consistent with a first-order transition. In fact, this point is a *multicritical* point. In the EHM, there is an intervening phase with long-range BOW for $U < U_m$.^{29,35,36} We find very similar behavior in the HHM except that the intervening phase here is the metallic intermediate state. We cannot calculate a precise value for U_m , but for $\omega=1$, it appears comparable ($U_m \sim 5$ for $\omega=1$) to the value found in the half-filled EHM, $U_m=4.7 \pm 0.1$.²⁹ We also remark that the change in the order of the transition may be related to discussions of quantum to classical crossover in e-ph coupled models.³⁷

D. Discussion of Luttinger exponents

In the LL picture, K_ρ and K_σ determine the asymptotic decay of correlation functions, and hence measurements of these exponents in finite systems have often been used to determine the phase diagrams of 1D models. Specifically, $K_\rho > 1$ corresponds to attractive charge correlations, while $K_\rho < 1$ corresponds to repulsive charge correlations. It is first instructive to review the LL exponents for the 1D Hubbard model and sources of error in finite-size systems. At half filling for $U > 0$, the 1D Hubbard model is insulating ($K_\rho=0$) with no spin gap ($K_\sigma=1$, spin rotational invariance holds). For $U < 0$, there is a spin gap ($K_\sigma=0$), and degenerate CDW and singlet superconducting (SS) pair correlations ($K_\rho=1$). Therefore, the LL exponents are *discontinuous* at $U=0$. The transition at $U=0$ is of the KT type, with the gaps (charge gap $U > 0$ or spin gap $U < 0$) opening exponentially slowly as U is varied from zero. In Fig. 7, we show K_ρ and K_σ for the 1D Hubbard model calculated using Eq. (21). There are two primary sources of finite-size error: first, the requirement that $q \rightarrow 0$ in Eq. (21), and second, the presence of logarithmic scaling corrections near a KT transition. The scaling with system size is slow close to the transition (U

$=0$) and particularly slow for the exponent that is expected to be equal to 1 (K_σ for $U > 0$ and K_ρ for $U < 0$). Such logarithmic scaling has been noted in other 1D electron and spin models and makes it difficult in practice to observe $K_\sigma = 1$ for the positive- U Hubbard model in a finite-size calculation.^{19,20} As discussed in Sec. III A, log corrections are expected to vanish exactly at critical coupling. In Fig. 7, this occurs at $U=0$, where K_ρ and K_σ curves for all system sizes cross at $K_\rho = K_\sigma = 1$.

Turning now to the HHM, the variation of K_σ for $g < g_{c1}$ [Fig. 5(b)] is consistent with log corrections in the spin degree of freedom that vanish at the spin-gap transition. This observation further reinforces our statement that the spin-gap transition is also of the KT type. For the K_ρ data in Fig. 4, K_ρ at $g=0$ is again exactly unity. K_ρ then crosses 1 from above at a g roughly consistent with the g_{c2} determined from the susceptibility data in Fig. 3. Assuming the Peierls transition occurs where $K_\rho = 1$ gives a critical coupling of $2g_{c2}^2\omega \approx 0.85$ after performing finite-size scaling using N up to 128 sites (Fig. 4). The form of the K_ρ plot for the HHM ($U=0$) is clearly similar to K_ρ for the negative- U Hubbard model (Fig. 7), with K_ρ starting at 1 for zero coupling and becoming slightly *larger* than 1 for nonzero coupling. While this apparent $K_\rho > 1$ may be interpreted as meaning that superconducting pair correlations are dominant,¹⁶ a more plausible interpretation is that the apparent $K_\rho > 1$ is a consequence of logarithmic scaling corrections. This implies that the true K_ρ should be exactly equal to unity for $g < g_{c2}$ and drop to zero for $g > g_{c2}$. This further implies that the intermediate state has *degenerate* CDW and SS correlations. This statement is consistent with our finding that the $U=0$ HHM for $g < g_{c2}$ has a spin gap but no charge gap.

Calculations for a model of acoustic phonons coupled to 1D electrons found that the LL expressions for decay of correlation functions must be modified due to retardation effects.²⁶ Specifically, the dominance of CDW and SS correlations is given by

$$K_\rho A \leq 1 \quad (\text{CDW}), \quad (22)$$

$$B/K_\rho \leq 1 \quad (\text{SS}), \quad (23)$$

where A and B depend on the strength of the e-ph coupling.²⁶ With zero e-ph coupling, $A=B=1$. For increasing e-ph coupling, $A > 1$ and $B < 1$, with A diverging and B approaching a finite value. The renormalized boundary for the metallic/Peierls transition is then $K_\rho = 1/A$. While there is no reason to expect that for the HHM model (with dispersionless phonons), the LL relations should be renormalized in the same manner, our SSE data may be consistent with $1/A$ slightly less than 1. Upon close examination of Figs. 4 and 3, the g_{c2} as determined by K_ρ crossing 1 is slightly smaller than the g_{c2} determined by susceptibility. The g_{c2} determined from K_ρ (Fig. 4) would coincide with the g_{c2} determined from $\chi_\rho(\pi)$ [Fig. 3(b)] if the horizontal line in Fig. 4 is moved slightly below 1, or $1/A \approx 0.95$.

For larger U , the size of the intermediate region shrinks, and K_ρ peaks at the transition, with K_ρ approaching 1 with increasing N [see Fig. 2(a) in Ref. 16, $U=2$, $\omega=0.5$]. The peak at the transition is consistent with $K_\rho = 0$ in the Mott and

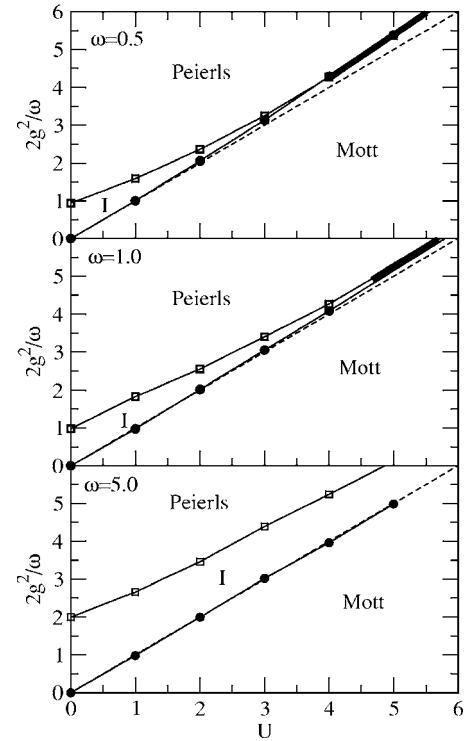


FIG. 8. Phase diagram of the half-filled HHM for $\omega=0.5$, $\omega=1$, and $\omega=5$. The dashed line is given by $U=2g^2/\omega$. All phase boundaries are determined using susceptibility and K_σ data, with uncertainty approximately the size of the symbols. Lines are guides to the eyes. The three phases shown are Mott, (I)ntermediate, and Peierls. The Mott/I and I/Peierls boundaries merge into a single first-order Mott/Peierls boundary indicated by a heavy line for $U \geq 4$ for $\omega=0.5$ and $U \geq 5$ for $\omega=1$.

Peierls states, and $K_\rho = 1$ only along their boundary. The apparent $K_\rho < 1$ at the peak may be due to the closer proximity to the first-order transition, where K_ρ drops quite rapidly to zero. For $U=2$ and $\omega=0.5$, we estimate that $0.95 \leq 1/A \leq 1$. If renormalization as in Ref. 26 does occur, for all parameter values we investigated, it appears that the effect is relatively small ($0.9 \leq A \leq 1$). Because measuring SS correlations is not practical in the SSE method, we cannot determine a value for B . Equation (23) with $B < 1$ would imply that SS correlations are dominant whenever K_ρ exceeds a value that is *smaller* than 1. SS is dominant for any nonzero e-ph coupling for $U=0$ in the calculation of Ref. 26, which seems unlikely in the HHM. We will discuss these implications further in Sec. V.

E. Phase diagram and half filling

In Fig. 8, we show the phase diagram for $\omega=0.5$, $\omega=1$, and $\omega=5$. All points were determined using susceptibility data for systems up to 32 (and in some cases 64 and 128) sites. We find that with increasing ω , the width of the intermediate region increases, and the tricritical point U_m moves to larger U . One further observation is that for $U \geq U_m$, the deviation of the Mott/Peierls boundary from $U_{\text{eff}}=0$ becomes noticeable, with the boundary shifting to $U_{\text{eff}} < 0$ (above the

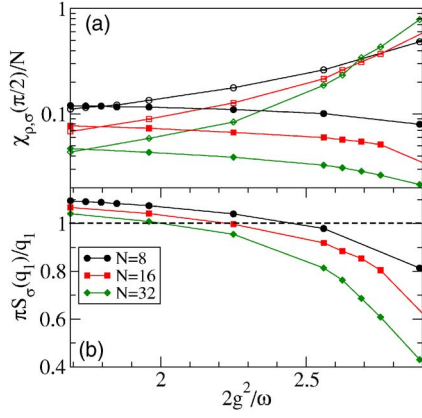


FIG. 9. (Color online) (a) Charge (open symbols) and spin (filled symbols) susceptibilities for the quarter-filled HHM with $U=2$, $\omega=0.5$. (b) Long-wavelength spin structure factor for the same parameters. We find similar behavior to half filling, Fig. 5, with first a transition to a spin-gapped state, and second, the transition to the Peierls CDW state.

dotted lines in Fig. 8). This shift can be seen, for example, in Fig. 6. For $U < U_m$, the Mott/intermediate spin-gap boundary is very close to the line $U_{\text{eff}}=0$.

IV. QUARTER FILLING

Many of the materials that the HHM is most applicable to are not half-filled. For example, most of the quasi-1D organic superconductors are $3/4$ filled ($1/4$ hole filled).¹ We therefore present some results for the HHM at quarter filling. Although for many of these materials it is necessary to include long-ranged Coulomb interactions (the extended Hubbard V term),³⁸ we will continue to focus on the HHM Hamiltonian with only on-site U and e-ph terms. We comment on the expected effect of V further below. As quarter filling is commensurate, a Peierls state is also expected to occur for sufficiently large g . There are, however, significant differences between half-filled and quarter-filled Peierls states. At quarter filling, there are more than one possible pattern of charge and bond distortion, and which one actually occurs depends on the values of U as well as V .^{39,40} In the absence of phonons, the quarter-filled band for finite U is a LL with neither charge nor spin gaps. At half filling, $\chi_\rho(2k_F)$ and $\chi_\sigma(2k_F)$ are degenerate at $U=0$ (note that $2k_F=\pi/2$ at quarter filling and corresponds to a correlation function with period 4 in real space). In the presence of phonons, we again expect the charge susceptibility $\chi_\rho(2k_F)/N$ to diverge.

Our SSE results show that the HHM at quarter filling is in many respects similar to the half-filled case. In Fig. 9, we show $\chi_\rho(2k_F)/N$ and $\pi S_\sigma(q_1)/q_1$ versus $2g^2/\omega$. We again find two transitions: first, a transition to a spin-gapped state, and second, the transition to the Peierls state. At half filling, the spin gap opens very close to the point where $U_{\text{eff}}=U-2g^2/\omega=0$. The phase diagram at quarter filling is therefore nearly identical to the phase diagram at half filling, with LL, intermediate, and Peierls phases. We find that the intermediate phase is slightly wider at quarter than half filling. For

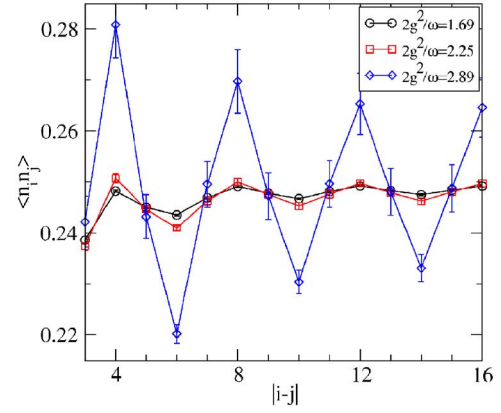


FIG. 10. (Color online) Charge-charge correlations $\langle n_i n_j \rangle$ versus distance $|i-j|$ for a 32 site quarter-filled system with $U=2$ and $\omega=0.5$. The three values of $2g^2/\omega=1.69$, 2.25 , and 2.89 correspond to LL, intermediate, and Peierls states, respectively. We find that in all three regions the charge correlations at quarter filling are of the form $\cdots 2000 \cdots$.

example, at quarter filling with $U=2$ and $\omega=0.5$ (Fig. 9), $2g_{c1}^2/\omega \approx 1.7$ and $2g_{c2}^2/\omega \approx 2.6$, compared to $2g_{c1}^2/\omega \approx 2.0$ and $2g_{c2}^2/\omega \approx 2.3$ at half filling. We note (see Fig. 9) that at quarter filling, we see slightly greater deviation from the $U_{\text{eff}}=0$ in the first (spin-gap) transition. At present, we do not have enough SSE data to investigate whether the tricritical point U_m occurs at half filling, but in our data at quarter filling, we do find that with increasing U , g_{c1} and g_{c2} become closer together. This suggests that a tricritical point also exists at quarter filling.

At quarter filling, there are two possible CDWs that are period 4 ($2k_F$). These have charge densities in cartoon form of either $\cdots 1100 \cdots$ or $\cdots 2000 \cdots$, where “1” or “2” indicates a charge density greater than the average density of 0.5 and “0” indicates a charge density less than the average.³⁹ The pattern $\cdots 2000 \cdots$ is found in the uncorrelated ($U=0$) band. In Fig. 10, we plot the real-space charge-charge correlation function $\langle n_i n_j \rangle$ versus distance $|i-j|$ for a range of g 's in the three phases. We find that the charge-charge correlation function peaks for sites separated by four lattice sites, consistent with a CDW state of the $\cdots 2000 \cdots$ form. The strength of the CDW correlations does not greatly change going from the LL to the intermediate phase, but increases rapidly after the Peierls transition. In the $\cdots 2000 \cdots$ CDW, the three small charges are not exactly equal, and the actual charge densities are in sequence large, medium, small, medium (LMSM). This charge pattern coexists with a BOW because L-M and M-S bonds are inequivalent. Figure 10 shows that the charge correlations follow this LMSM pattern as expected. We conclude that the pairing at quarter filling in the HHM consists of on-site electron pairs as found at half filling, at least for the small through intermediate U we have currently investigated.

The distinction between these two CDW patterns at quarter filling is important because while $\cdots 2000 \cdots$ is related to *on-site* electron pairs, the more extended CDW $\cdots 1100 \cdots$ is related to *nearest-neighbor* pairing. The $\cdots 1100 \cdots$ requires bond-coupled phonons in addition to the Holstein phonons

considered here.^{39,40} In addition, the pattern of the BOW (the location of the “strong” bond) coexisting with the $\cdots 1100 \cdots$ CDW also depends on the strength of V .³⁹ If a similar metallic phase exists adjacent to the $\cdots 1100 \cdots$ CDW, it is possible that a region of nearest-neighbor superconducting pairing found may be relevant to real quarter-filled molecular superconductors.

V. CONCLUSIONS

To summarize, we have presented numerical data for charge and spin correlations of the 1D HHM model at half and quarter filling. We have based our phase diagram on charge and spin susceptibilities, which provide direct indication of phase boundaries with much weaker finite-size effects than previous calculations based on LL exponents.¹⁶ We find that the spin-gap and Peierls transitions do not occur simultaneously unless U is larger than a critical U_m . For $U < U_m$, as the e-ph coupling is increased from zero, the spin gap opens *before* the Peierls state forms. The intermediate state is metallic with a spin gap but no charge gap, and the transitions to and from the intermediate state are of the KT type. Our physical picture of the intermediate state is that at the spin-gap transition (g_{c1}), pairs are formed, but are disordered and do not order in a Peierls state until the e-ph coupling is further increased. For $U > U_m$, the two transitions merge into a single first-order Mott/Peierls transition. With finite-size calculations, we cannot completely discount the possibility of a small charge gap (small compared to the finite-size gap) in the intermediate region. However, finite charge stiffness (Drude weight) provides further evidence for metallic behavior in the intermediate state.¹⁶

Compared to other calculations, the critical coupling we determined for g_{c2} at $U=0$ is consistent with previous results.^{10,11} The variational results of Ref. 15 find the intermediate phase existing in a narrow region on both sides of the $U_{\text{eff}}=0$ line, while we find the intermediate phase only for $U_{\text{eff}} < 0$. Several calculations of the single-particle spectral function are available for the HHM,^{41–43} the spinless Holstein model,^{44,45} as well as the $d=\infty$ studies previously mentioned. In Ref. 42, using a cluster perturbation theory method applied to the 1D HHM, a small nearly dispersionless peak was found in the spectral function for small k . This small peak is also found in the spectral function of the metallic phase of the spinless Holstein model and may possibly be associated with the intermediate phase.

Considering the possible modification of the LL equations in the presence of retarded e-ph interactions, we find that while this could possibly occur in a form that would agree with Ref. 26 the amount of renormalization is small ($1/A \sim 0.95$), and possibly within finite-size errors in our determination of the transition points. We also do not see any measurable or consistent change in the constant A when comparing $\omega=0.5$ and $\omega=1$, which would be expected to change the amount of retardation in the e-ph interaction. We are not able to calculate a value for B in Eq. (23). However, if Eq. (23) is correct for the HHM model with $B < 1$, SS correlations would actually be *enhanced* because of retardation.²⁶

An important question is the strength of SS correlations within the intermediate region. In terms of the LL framework, models with $K_\rho > 1$ have dominant superconducting correlations. Indeed, our numerical data appear to show $K_\rho > 1$ in the intermediate region, but this result is likely to be a finite-size effect. If we set aside any renormalization of K_ρ , our conclusion based on comparison with the 1D negative- U Hubbard model is that in the intermediate region, K_ρ is *exactly* equal to 1. This implies that in the intermediate region, CDW and SS correlations are, in fact, *exactly degenerate*. This exact degeneracy may not be easily observable in a finite system due to the finite-size difficulties near KT transitions. As the SSE method is based on a world-line approach in imaginary time, there is no simple way to measure correlations involving four particles, which would be needed to measure SS correlations directly. Density matrix renormalization group (DMRG) (Ref. 27) calculations suggest that while SS and CDW correlations are nearly degenerate in the intermediate region, CDW correlations appear slightly stronger at long range. DMRG results for a ladder system suggest that going beyond 1D can break the degeneracy, giving a region with dominant SS correlations.²⁷ Finally, we remark that in addition to the logarithmic scaling difficulties, observing metallic behavior in close proximity to a CDW is difficult due to the typically rapidly increasing autocorrelation time for QMC methods. We do find in our method that the autocorrelation time τ increases rapidly close to the Peierls boundary, but believe that the use of parallel tempering can reduce τ enough to obtain reliable results.

ACKNOWLEDGMENTS

The authors acknowledge support of American Chemical Society Petroleum Research Fund and the Department of Energy Grant No. DE-FG02-06ER46315.

*Electronic address: r.t.clay@msstate.edu

¹T. Ishiguro, K. Yamaji, and G. Saito, *Organic Superconductors* (Springer-Verlag, New York, 1998).

²O. Gunnarsson, *Rev. Mod. Phys.* **69**, 575 (1997).

³T. Holstein, *Ann. Phys. (N.Y.)* **8**, 325 (1959).

⁴J. Hubbard, *Proc. R. Soc. London, Ser. A* **276**, 238 (1963).

⁵R. E. Peierls, *Quantum Theory of Solids* (Clarendon, Oxford, 1955).

⁶E. H. Lieb and F. Y. Wu, *Phys. Rev. Lett.* **20**, 1445 (1968).

⁷J. E. Hirsch and E. Fradkin, *Phys. Rev. Lett.* **49**, 402 (1982).

⁸J. E. Hirsch and E. Fradkin, *Phys. Rev. B* **27**, 4302 (1983).

⁹R. J. Bursill, R. H. McKenzie, and C. J. Hamer, *Phys. Rev. Lett.* **80**, 5607 (1998).

¹⁰C. Q. Wu, Q. F. Huang, and X. Sun, *Phys. Rev. B* **52**, R15683 (1995).

¹¹E. Jeckelmann, C. Zhang, and S. R. White, *Phys. Rev. B* **60**, 7950

- (1999).
- ¹²D. Meyer, A. C. Hewson, and R. Bulla, *Phys. Rev. Lett.* **89**, 196401 (2002).
- ¹³M. Capone, G. Sangiovanni, C. Castellani, C. D. DiCastro, and M. Grilli, *Phys. Rev. Lett.* **92**, 106401 (2004).
- ¹⁴W. Koller, D. Meyer, and A. C. Hewson, *Phys. Rev. B* **70**, 155103 (2004).
- ¹⁵Y. Takada and A. Chatterjee, *Phys. Rev. B* **67**, 081102(R) (2003).
- ¹⁶R. T. Clay and R. P. Hardikar, *Phys. Rev. Lett.* **95**, 096401 (2005).
- ¹⁷A. W. Sandvik, *J. Phys. A* **25**, 3667 (1992).
- ¹⁸A. W. Sandvik, *Phys. Rev. B* **59**, R14157 (1999).
- ¹⁹A. W. Sandvik and D. K. Campbell, *Phys. Rev. Lett.* **83**, 195 (1999).
- ²⁰P. Sengupta, A. W. Sandvik, and D. K. Campbell, *Phys. Rev. B* **67**, 245103 (2003).
- ²¹O. F. Syljuasen and A. W. Sandvik, *Phys. Rev. E* **66**, 046701 (2002).
- ²²A. W. Sandvik, R. R. P. Singh, and D. K. Campbell, *Phys. Rev. B* **56**, 14510 (1997).
- ²³H. J. Schulz, in *Low-Dimensional Conductors and Superconductors*, edited by D. Jérôme and L. G. Caron (Plenum, New York, 1987), p. 95.
- ²⁴J. Voit, *Rep. Prog. Phys.* **58**, 977 (1995).
- ²⁵R. T. Clay, A. W. Sandvik, and D. K. Campbell, *Phys. Rev. B* **59**, 4665 (1999).
- ²⁶D. Loss and T. Martin, *Phys. Rev. B* **50**, 12160 (1994).
- ²⁷M. Tezuka, R. Arita, and H. Aoki, *Phys. Rev. Lett.* **95**, 226401 (2005).
- ²⁸K.-M. Tam, S.-W. Tsai, D. K. Campbell, and A. H. Castro Neto, *Phys. Rev. B* **75**, 161103(R) (2007).
- ²⁹P. Sengupta, A. W. Sandvik, and D. K. Campbell, *Phys. Rev. B* **65**, 155113 (2002).
- ³⁰E. Fradkin and J. E. Hirsch, *Phys. Rev. B* **27**, 1680 (1983).
- ³¹L. G. Caron and S. Moukouri, *Phys. Rev. Lett.* **76**, 4050 (1996).
- ³²J. E. Hirsch, *Phys. Rev. Lett.* **53**, 2327 (1983).
- ³³J. W. Cannon and E. Fradkin, *Phys. Rev. B* **41**, 9435 (1990).
- ³⁴J. W. Cannon, R. T. Scalettar, and E. Fradkin, *Phys. Rev. B* **44**, 5995 (1991).
- ³⁵M. Nakamura, *J. Phys. Soc. Jpn.* **68**, 3123 (2000).
- ³⁶M. Nakamura, *Phys. Rev. B* **61**, 16377 (2000).
- ³⁷L. G. Caron and C. Bourbonnais, *Phys. Rev. B* **29**, 4230 (1984).
- ³⁸J. Hubbard, *Phys. Rev. B* **17**, 494 (1978).
- ³⁹K. C. Ung, S. Mazumdar, and D. Toussaint, *Phys. Rev. Lett.* **73**, 2603 (1994).
- ⁴⁰R. T. Clay, S. Mazumdar, and D. K. Campbell, *Phys. Rev. B* **67**, 115121 (2003).
- ⁴¹H. Fehske, G. Wellein, G. Hager, A. Weisse, and A. R. Bishop, *Phys. Rev. B* **69**, 165115 (2004).
- ⁴²W.-Q. Ning, H. Zhao, C. Q. Wu, and H.-Q. Lin, *Phys. Rev. Lett.* **96**, 156402 (2006).
- ⁴³H. Matsueda, T. Tohyama, and S. Maekawa, *Phys. Rev. B* **74**, 241103(R) (2006).
- ⁴⁴M. Hohenadler, G. Wellein, A. R. Bishop, A. Alvermann, and H. Fehske, *Phys. Rev. B* **73**, 245120 (2006).
- ⁴⁵S. Sykora, A. Hübsch, and K. W. Becker, *Europhys. Lett.* **76**, 644 (2006).